Table I. Esr Spectral Parameters

	Ascorbic acid[a]	Arabo-ascorbic acid[a]	α-Hydroxy-tetronic acid[a]	γ-Methyl-α-hydroxy-tetronic acid
g factor[b]	2.00518	2.00519	2.00519	2.00519
$a(H_4)$[c]	1.76	1.84	2.32	1.84
$a(H_5)$	0.07	<0.04		0.05
$a(C_1)$	5.74	5.70	5.72	5.69
$a(C_3)$	3.62	3.72	3.65	3.54
$a(C_2)$	0.96	0.92	1.03	0.91
$a(C_4)$	2.78	2.62	2.85	2.76
$a(C_5)$	*d*	*d*		<0.8

[a] From ref 2. [b] The *g* factors are known with an absolute accuracy of 0.00003 and relative to each other with an accuracy of 0.00001. [c] The hyperfine constants are accurate to 0.02 G. [d] The previous assignment of hyperfine constants of ~2.3 G to the C_5 carbon atoms (ref 2) now appears to be incorrect by virtue of the fact that no such constant is observed in the present case.

present in the γ-methyl-α-hydroxytetronic acid system has the structure

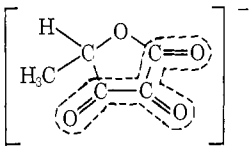

II

with the unpaired electron being delocalized in the tricarbonyl system.

Radical II can be produced from the parent anion by OH attack either directly by electron transfer to the OH radical or indirectly by addition of the OH to the double bond at either the C_2 or C_3 position followed by loss of water, *i.e.*

$$\cdot OH + I \longrightarrow II + H_2O \quad (1)$$

Pulse radiolysis experiments[10] show that for ascorbic acid reaction 1 is complete within a millisecond.

The protonation of radical I was examined by determining the pH dependence of the *g* factor and proton hyperfine constant and the results are illustrated in Figure 2. These parameters are independent of pH above pH 2. Studies were carried out in more acidic solutions (to solutions 6 *M* in $HClO_4$). The detailed interpretation of these results is somewhat more simple than those for the ascorbic acid system, since the additional structure resulting from the protons on the C_6 position is absent. The *g* factor of the protonated form of the radical is estimated as 2.00472, and the hyperfine constant of the C_4 proton as 0.14 G (compared with the estimates[2] of 2.00482 and 0.16 G in the ascorbic acid case). The p*K* for the protonation of radical I is −0.40.

(10) M. Schöneshöfer, *Z. Naturforsch. B*, **27**, 649 (1972).

Electronic Structure and Spectroscopy of Parabanic Acids[1]

Donald B. Larson, John F. Arnett, and S. P. McGlynn*

Contribution from the Coates Chemical Laboratories, The Louisiana State University, Baton Rouge, Louisiana 70803. *Received April 16, 1973*

Abstract: The four lowest energy excited electronic states of parabanic acid and three of its alkyl derivatives have been characterized by means of empirical generalizations, CNDO/s–CI computational results, and a composite-molecule analysis of the acid in terms of its oxamide and carbonyl residues. The lowest energy $S_i \leftarrow S_0$ transitions are assigned, in order of increasing energy as $^1B_2 \leftarrow {}^1A_1$ ($^1\Gamma_{n_+\pi_+^*} \leftarrow {}^1\Gamma_1$), $^1B_1 \leftarrow {}^1A_1$ ($^1\Gamma_{\pi_\ominus\pi_+^*} \leftarrow {}^1\Gamma_1$), and $^1A_1 \leftarrow {}^1A_1$ ($^1\Gamma_{\pi_\oplus\pi_+^*} \leftarrow {}^1\Gamma_1$). The luminescence of parabanic acid and methylparabanic acid is assigned as $^3B_2 \rightarrow {}^1A_1$ ($^3\Gamma_{n_-\pi_+^*} \rightarrow {}^1\Gamma_1$). The luminescence of the dialkyl derivatives of parabanic acid involves decay of an excited state of mixed $^3\Gamma_{n\pi^*}/{}^3\Gamma_{\pi\pi^*}$ character. The drastic change of emissive characteristics caused by dialkylation is attributed to a decrease of the $^3\Gamma_{n\pi^*}/{}^3\Gamma_{\pi\pi^*}$ energy gap. Finally, a composite-molecule analysis indicates that the T_1 state of all parabanic acids is highly localized on the dicarbonyl residue, a prediction substantiated by vibronic analyses of the phosphorescence spectra.

A large group of molecules is related, at least in a formal sense, by the presence of —C(=O)N< units bonded directly to identical units or to such functional units as >C=O, —N<, >C=C, etc. Included in this group are urea, oxamide, parabanic acid, alloxan, barbituric acid, and uric acid. It has been shown[2] that a useful interpretation of the absorption and emission characteristics of oxamides, >N–CO–CO–N<, in terms of amide properties may be obtained using a composite-molecule analysis of CNDO/s–CI computational results. The formal similarity of parabanic acid (imidazolidinetrione) and *cis*-oxamide suggests that a composite-molecule analysis of the more complex molecule can also lead to useful results.

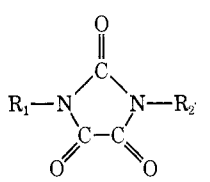

The following derivatives were studied (R_1, R_2, acronym): parabanic acid (H, H, PA); methylparabanic acid (CH_3, H, MPA); dimethylparabanic acid (CH_3, CH_3, DMPA); di-*n*-propylparabanic acid (C_3H_7, C_3H_7, DPPA).

(1) This work was supported by contract between the United States Atomic Energy Commission-Biology Branch and The Louisiana State University.

(2) D. B. Larson and S. P. McGlynn, *J. Mol. Spectrosc.*, in press.

Table I. Absorption Data for PA and Its Alkyl Derivatives

Compd	Solvent: Ethanol λ_{max}, mμ	Ethanol ϵ_{max}, M^{-1} cm^{-1}	Water λ_{max}, mμ	Acetonitrile λ_{max}, mμ	Acetonitrile ϵ_{max}, M^{-1} cm^{-1}	Ether λ_{max}, mμ	Ether ϵ_{max}, M^{-1} cm^{-1}	MCH[c] λ_{max}, mμ
PA	310	58.6	298	312	59.9	316.0	54.3	
	~248[a]	1500	~247[a]	~248	1400	~245[a]		
	212	13200	211	210	13200	210.0		
MPA	307	63.2	~307[a]	310	68.5	315.5	57.6	
	~255[a]	1220	258	253		253[a]		
	215	13000	215	214		213.0		
DMPA	~313[a]	60.0	*b*	~310[a]	90.2	314.0	66.8	320
	260	733	264.5	263		256		260
	218	12300	218.5	218		217.0		218[d]
DPPA	~315[a]	61.4	*b*	~310[a]	80.5	316.0	57.9	321
	263[a]	541	267.5	~263		257		259
	220	10100	221.0	219.5		219.3		220

[a] Shoulder. [b] No band detectable. [c] Methylcyclohexane. [d] Methylpentane.

In the course of this investigation, it become apparent that the parabanic acid systems possessed certain properties that are interesting in their own right. Dialkylation of PA, for example, produces a dramatic change of emission characteristics. A few other systems are known to undergo[3] drastic changes of emission properties upon relatively small perturbations (*i.e.*, solvent changes or alkylation) and these effects have been associated with the presence of close lying $^3\Gamma_{n\pi^*}$ and $^3\Gamma_{\pi\pi^*}$ states. A similar interpretation provides an equally adequate rationalization of the parabanic acid phenomenology.

Experimental Section

PA (Aldrich) was purified by repeated crystallization from water. The alkylparabanic acids were prepared by the reaction in anhydrous ether of equimolar quantities of the appropriately N-substituted urea with oxalyl chloride in the presence of sodium carbonate. Methylurea (Matheson Coleman and Bell) and 1,3-dimethylurea (Eastman) were commercial products; 1,3-di-*n*-propylurea was prepared by the reaction of *n*-propylamine and phosgene in anhydrous ether. The derivatives of PA were purified by recrystallization from ethanol and their physical constants follow.

Anal. Calcd for $C_4H_4O_3N_2$: C, 37.7; H, 3.14; N, 21.8. Found: C, 37.6; H, 3.17; N, 22.2.

DMPA: mp 148–149° (from EtOH) [lit.[4] 149–150°].

Anal. Calcd for $C_5H_6O_3N_2$: C, 42.2; H, 4.20; N, 19.8. Found: C, 41.8; H, 4.24; N, 19.8.

DPPA: mp 44.5–45.5° (from EtOH).

Anal. Calcd for $C_9H_{14}O_3N_2$: C, 54.5; H, 5.75; N, 14.1. Found: C, 54.5; H, 6.41; N, 14.3.

Instrumentation and techniques were the same as those described previously.[2] Relative emission quantum yields were estimated by comparing the luminescence intensities of solutions of equal absorptivity at 315 mμ.

Results

Absorption. The low-energy electronic absorption spectra of PA and its derivatives are shown in Figure 1. Three distinct absorption regions are apparent and each of these behaves quite differently upon alkyl substitution.

(i) Region I extends from 350 to 295 mμ and exhibits weak absorption (ϵ_{max} ~65 M^{-1} cm^{-1}). Region I absorption is well defined in PA but deteriorates to a shoulder in all the other derivatives, being much less distinct for the dialkyl derivatives than for MPA. Nonetheless, with the single exception of DMPA which onsets at 340 mμ, region I absorptions all initiate in the interval 350–345 mμ.

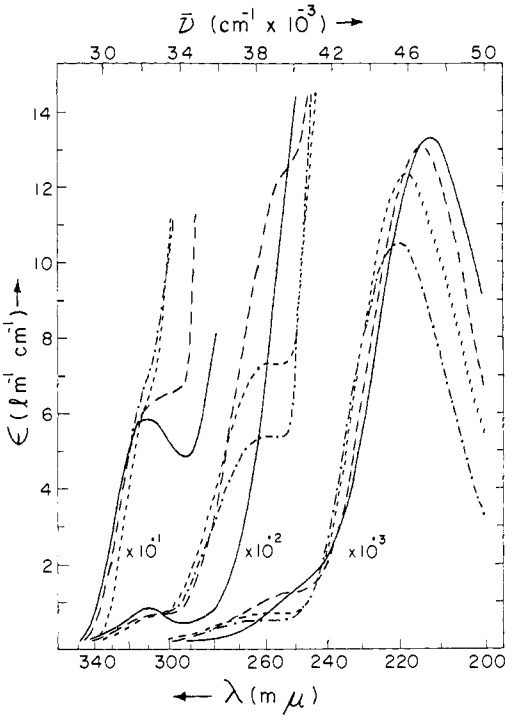

Figure 1. Absorption of PA and its alkyl derivatives in ethanol: (——) PA, (– – –) MPA, (- - - - - -) DMPA, (—·—) DPPA.

(ii) Region II encompasses the interval 300 to 240 mμ and is characterized by moderate absorptivities (ϵ_{max} ~500–1500 M^{-1} cm^{-1}). Region II absorptivity exhibits the largest intensity changes. The intensity, as well as the energy of the absorption maximum, decreases with increasing alkylation in the order PA > MPA > DMPA > DPPA. A comparison of PA and DPPA indicates a red shift of ~10 mμ and a decrease in maximum intensity of ~60%.

(iii) Region III extends from 240 to 200 mμ and exhibits intense absorption (ϵ_{max} ~10500–13500 M^{-1} cm^{-1}). Region III maxima are well defined and their behavior is very similar to that of the absorptions of region II. The extreme red shift is 8 mμ and the intensity decrease is ~25%.

The effects of different solvents on the absorptivities of regions I–III are summarized in Table I.

(3) For example, see R. M. Hochstrasser and C. Marzzacco, *J. Chem. Phys.*, **49**, 971 (1968); A. A. Lamola, *ibid.*, **47**, 4810 (1967).

(4) J. Beilstein, "Handbuch der Organischen Chemie," 1st ed, Vol. 24, Julius Springer, Berlin, Germany, 1936, pp 402–404.

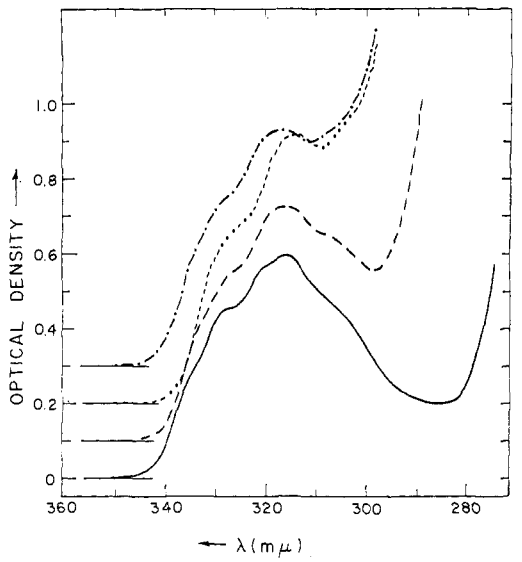

Figure 2. Lowest energy absorption of PA and its alkyl derivatives in ether: (——) PA, (– – –) MPA, (- - - - - -) DMPA, (—·—) DPPA. The zero absorptivity base line is displaced vertically for greater clarity.

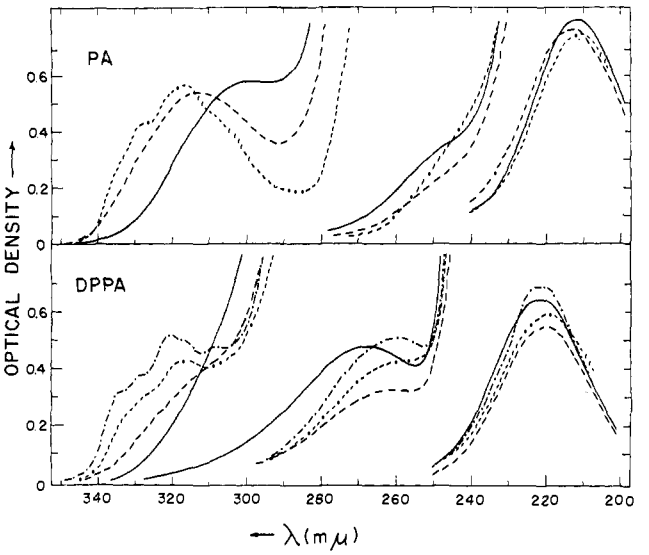

Figure 3. Solvent perturbations on the electronic absorption of PA and DPPA: (——) water, (– – –) ethanol, (- - - - - -) ether, (—·—) methylcyclohexane.

Region I is better examined in ether solution (Figure 2), where the band is fairly well defined for all compounds. For PA, the absorption is almost completely separated from the more intense region II absorption and exhibits the most vibrational structure. The onsets and maxima of absorption blue shift and the ϵ_{max} values increase in a regular order from PA to DMPA; however, these trends reverse for DPPA. On the other hand, all maxima are located at ~316 mμ and the ϵ_{max} values are similar for all except DMPA. Regardless of the correlation adopted, region I absorption characteristics are still quite similar for all compounds.

The comparative behavior of the three absorption regions in various solvents also reveals different patterns. These are illustrated in Figure 3 for PA and DPPA. The solvent shift behavior of region I is most obvious in PA because the long wavelength absorption band is clearly resolved in all solvents. A change of solvent from ether to water produces a loss of vibrational structure and a blue shift of ~18 mμ in the absorption maximum. Similar effects occur in DPPA except that no inflection at all is detectable in aqueous solutions; in addition, the better solubility properties of DPPA allow a study of region I in a hydrocarbon solvent.

Five vibrational bands are discernible in region I for DPPA in methylcyclohexane solution (see Figure 3). An analysis of this system is given in Table II; it consists of two progressions in a ~1260-cm^{-1} vibrational mode initiating in origins at 334.5 (29,895) and 329.0 mμ (30,395 cm^{-1}). From the analysis of the ir and Raman spectra of PA,[4] the ~1260-cm^{-1} interval is attributed to an excited-state symmetric carbonyl stretching mode and the ~500-cm^{-1} separation between the two origins to a nontotally symmetric carbonyl in-plane bending mode. Both values are ~70% of the corresponding frequencies reported[5] for the ground state.

(5) A. Alemagna and V. Lorenzelli, *J. Chim. Phys.*, 61, 884 (1964).

Table II. Analysis of Region I Absorption of DPPA in Methylcyclohexane Solution

Wavelength, mμ	Energy, cm^{-1}	Δ, cm^{-1}		Assignment,[a] ν_1,ν_2
334.5	29900	0	0	0,0
329.0	30400		500	1,0
321.0	31150	1250		0,1
316.5	31600		1200	1,1
308.0	32470	1320		0,2

[a] ν_1 = 525 cm^{-1} and ν_2 = 1260 cm^{-1}.

A similar analysis also applies to PA in ether solution; in fact, the vibronic energies recorded for DPPA are more or less identical with those of PA (see Figure 3), except that the fourth vibronic band (1,1) is the most intense for PA while the third band (0,1) is found to be most intense in DPPA. However, this comparison contrasts PA in ether with DPPA in methylcyclohexane and, therefore, the reversal of intensities could be due either to solvent effects or to alkylation changes. An examination of DPPA in mixed solvents progressing from 3-methylpentane to ether indicates that it is the change in solvent which causes the reversal in intensities. The 0,0 and 0,1 bands are preferentially decreased in intensity and the 1,0 and 1,1 bands are intensified, leading to a change in λ_{max} from the 0,1 band in hydrocarbon solvent to the 1,1 band as found in ether. Thus, based on λ_{max} values, a larger blue shift is estimated to occur in the polar solvent than is found by direct comparison of vibronic band positions.

The absorption of region II for PA is ill resolved, the best definition occurring in aqueous solutions where the band is located at ~245 mμ (see Figure 3). For DPPA, on the other hand, this region exhibits relatively well-defined maxima in all solvents and these maxima are substantially red shifted relative to PA (for aqueous solutions, for example, the red shift is ~23 mμ). This absorption region also shows distinct solvent red shifts in going from noninteracting

Table III. Analysis of Emission Spectrum of PA in EPA at 77°K

Wavelength, mμ	Energy, cm⁻¹	Δ, cm⁻¹		Assignment,[a] ν₁,ν₂
357.0	28010	0	0	0,0
365.0	27400	610		1,0
381.2	26230		1780	0,1
390.5	25610	1790		1,1
407.2	24560		1770	0,2
420.0	23810	1800		1,2
438.5	22810		1750	0,3

[a] $\nu_1 = 630\,cm^{-1}$ and $\nu_2 = 1780\,cm^{-1}$.

to strongly interacting solvents (*i.e.*, a red shift of ~9 mμ for the change from methylcyclohexane to water).

Both compounds exhibit slight solvent shifts of region III and an apparent vibrational structure becomes marginally detectable in some solvents. The absorption maxima of the alkylated derivatives all lie to the red of those for PA.

Emission. PA and its alkyl derivatives are emissive at 77°K (see Figure 4) when excited in the lowest energy absorption band. The separation of absorption and emission origins is small (<4000 cm^{-1}) in all cases. However, the emissions of PA and MPA are distinctly different from those of DMPA and DPPA.

PA exhibits an intense luminescence for which the decay time at 77°K is ~1.5 msec. The emission is structured and the seven bands resolved in EPA may be analyzed as two progressions in an interval of ~1780 cm^{-1} as shown in Table III: one progression originates at 357.0 mμ (28,010 cm^{-1}) and the other at 365 mμ (28,010 − 610 cm^{-1}). The two active frequencies, 1780 and 630 cm^{-1}, are readily assigned[5] as a carbonyl stretching mode and a nontotally symmetric carbonyl in-plane bending mode, respectively.

The emission of MPA is shown in Figure 4. It is structured much like that of PA but is blue shifted by ~3.5 mμ. The lifetime of this emission in EPA is slightly longer than that of PA and the quantum yield, while comparable to that of PA, is less.

The emission profiles of the two dialkylated derivatives are quite different from those of PA and MPA as shown in Figure 4. The vibronic bands are ill resolved and the dominant vibrational mode possesses a frequency of ~1450 cm^{-1}. The emissive decay times are about ten times longer and the relative quantum yields about ten times smaller than those of PA and MPA (*i.e.*, the natural lifetime has increased by a factor of ~100 in the dialkyls).

The emission–excitation maxima of PA and DPPA are similar to the lowest energy bands found in the corresponding absorption spectra in EPA at 77°K. No substantial solvent shift is found for the emissions in EPA relative to those in mixed alcohol glasses (Table IV). However, for DPPA, a red shift of ~7 mμ is found in 3-MP and ~9 mμ in the crystal relative to EPA or mixed alcohol solutions.

Theoretical. The results of CNDO/s computations[6] are given in Figure 5 in the form of an MO

(6) The CNDO/s-CI program was obtained from the Quantum Chemistry Program Exchange (QCPE 174). Only the first 30 monoexcited configurations were included in the CI routine. Bond lengths and bond angles for PA were those of D. R. Davies and J. J. Blum, *Acta Crystallogr.*, 8, 129 (1955). Standard structural parameters were used for the $-CH_3$ groups of the PA derivatives.

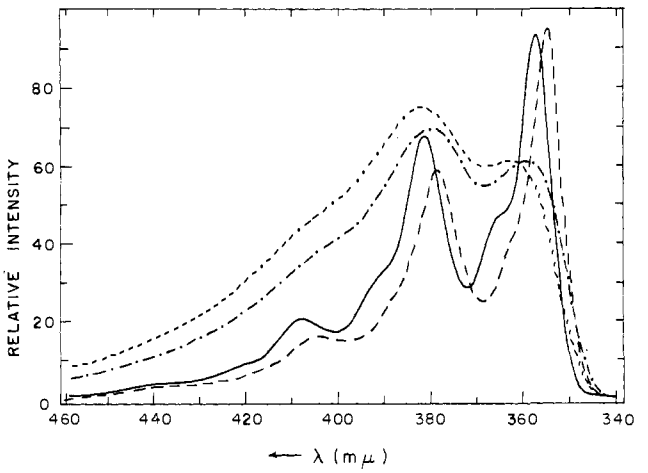

Figure 4. Emission spectra of PA and its alkyl derivatives in EPA at 77°K: (——) PA, (– – –) MPA, (- - - - - -) DMPA, (—·—) DPPA.

Table IV. Emission Data for PA and Its Alkyl Derivatives at 77°K

Compd	Solvent	λ_{max}^{em}, mμ 1st band	2nd band	λ_{max}^{exc}, mμ	τ, msec
PA	EPA[a]	357.0	380.6	324 (323[b])	1.5
	Mixed alc[c]	357.0	380.0		1.8
MPA	EPA	353.5	377.0	322	2.4
	Mixed alc	354.0	377.4		2.6
DMPA	EPA	364.0	382.0	312	27
	Mixed alc	364.0	383.0		15
	3-MP[d]				24
DPPA	EPA	358.4	379.0	318 (318[b])	10
	Mixed alc	360.0	381.0		15
	3-MP	367.6	390.0		13
	Crystalline solid	369.0	392.0		

[a] Mixture of ether, isopentane, and ethanol. [b] λ_{max} derived from 77°K absorption in EPA. [c] Mixture of methyl, ethyl, and isopropyl alcohols. [d] 3-Methylpentane.

correlation diagram. The highest energy filled MO of PA, $n_3(9a_1)$, is classified as a nonbonding σ MO; it is localized on the dicarbonyl oxygens but possesses significant σ-bonding character across the carbonyl–carbonyl bond. The other n orbitals lack this latter chracteristic. The $n_2(7b_1)$ MO is highly localized on the isolated carbonyl portion of PA, while the $n_1(6b_1)$ orbital has contributions at all three oxygens. The highest energy filled π MO, $\pi_5(3b_2)$, contains significant contributions only at the two nitrogen and three oxygen centers and is classified as a nonbonding π MO. The $\pi_4(2a_2)$ MO is similarily classified as nonbonding except that it possesses no amplitude on the isolated carbonyl centers. As in the case of π_4, $\pi_3(1a_2)$ contains no isolated carbonyl contributions; however, the π_3 MO is bonding in the N–C–O regions and, at the same time, antibonding across the carbon–carbon bond. The $\pi_2(2b_2)$ MO is bonding at all carbon–oxygen bonds and possesses insignificant amplitudes at the nitrogen centers; it is, however, bonding in the carbon–carbon bond region. The totally symmetric π_1 MO (not shown) is much more bonding than the MO's of Figure 5. The σ MO's with the sole exception of the $\sigma(8a_1)$ MO located at −15.7 eV, are all at substantially lower energies than the MO's of Figure 5.

Table V. CNDO/s–CI Results for the Three Lowest Energy Transitions of PA and Its Methyl Derivatives[a]

	Transition								
	$^1B_2 \leftarrow {}^1A_1$ ($^1\Gamma_{n_+\pi_+^*} \leftarrow {}^1\Gamma_1$)			$^1B_1 \rightarrow {}^1A_1$ ($^1\Gamma_{\pi_\ominus\pi_+^*} \leftarrow {}^1\Gamma_1$)			$^1A_1 \leftarrow {}^1A_1$ ($^1\Gamma_{\pi_\ominus\pi^{+*}} \leftarrow {}^1\Gamma_1$)		
Compd	Energy, eV	f no.[b]	CI compn[c]	Energy, eV	f no.	CI compn[c]	Energy, eV	f no.	CI compn[c]
PA	2.76		85% $n_3\pi_6^*$	6.72	0.05	90% $\pi_4\pi_6^*$	6.86	0.34	98% $\pi_5\pi_6^*$
MPA[d]	2.74		85% $n_3\pi_6^*$	6.83	0.28	70% $\pi_4\pi_6^*$ 23% $\pi_5\pi_6^*$	6.30	0.11	70% $\pi_5\pi_6^*$ 27% $\pi_4\pi_6^*$
DMPA	2.72		85% $n_3\pi_6^*$	6.15	0.03	90% $\pi_4\pi_6^*$	6.53	0.36	98% $\pi_5\pi_6^*$

[a] See Figure 8 and related text for explanation of notation. [b] The $^1B_2 \leftarrow {}^1A_1$ transition is dipole allowed. The oscillator strengths of dipole-allowed $\pi^* \leftarrow$ n transitions are improperly normalized to zero in all CNDO/s formulations. [c] The CI composition of MPA and DMPA states is expressed using the MO notation appropriate for PA (see Figure 5). [d] This molecule is of C_s symmetry. Consequently, all $^1\Gamma_{n\pi^*} \leftarrow {}^1\Gamma_1$ transitions are allowed and are designated as $^1A'' \leftarrow {}^1A'$. All $^1\Gamma_{\pi\pi^*} \leftarrow {}^1\Gamma_1$ transitions are designated as $^1A' \leftarrow {}^1A'$. Correlation with transitions of C_{2v} molecules is made on the basis of the MO correlations of Figures 5 and 6.

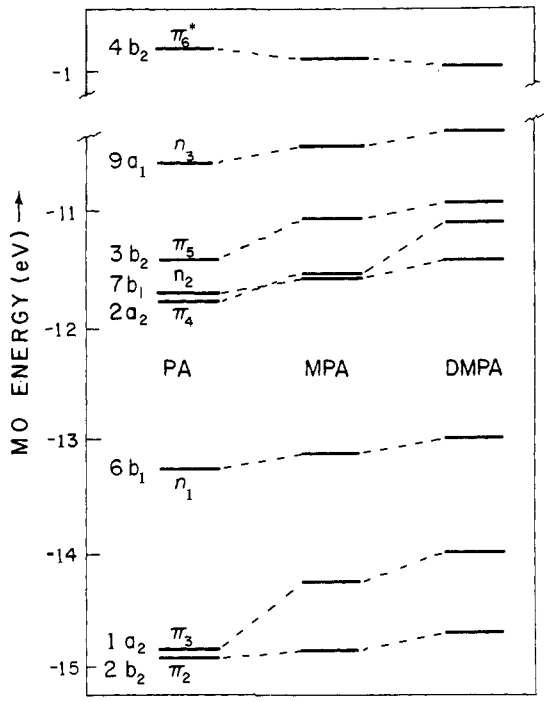

Figure 5. MO correlation diagram of CNDO/s–CI results for PA and its methyl derivatives.

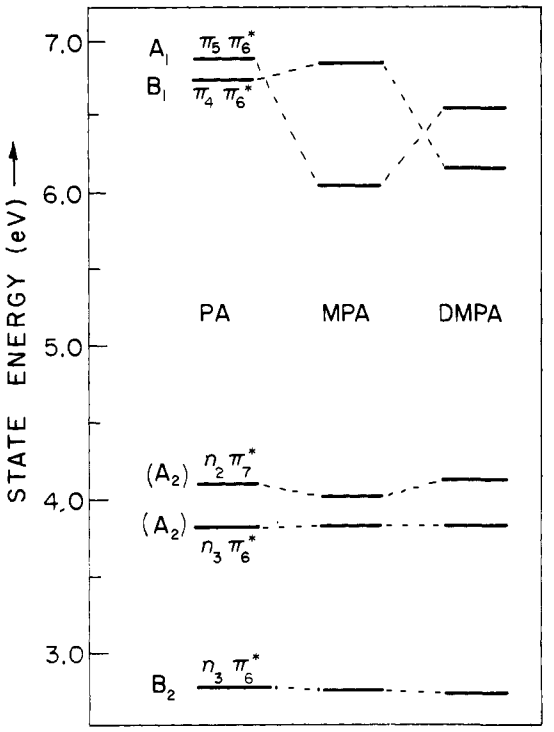

Figure 6. State correlation diagram of CNDO/s–CI results for PA and its methyl derivatives. Those states involved in symmetry-forbidden electric-dipole transitions with the ground state are given in parentheses. $^1\Gamma_{n\pi^*}$ states calculated at energies greater than the lowest $^1\Gamma_{\pi\pi^*}$ state are not included.

The three lowest energy virtual orbitals are all of π symmetry. The lowest energy unfilled MO is $\pi_6^*(4b_2)$; it exhibits an electron distribution similar to that of the $\pi_2(1b_2)$ MO (*i.e.*, negligible density at the nitrogens) except that now the largest MO coefficients are located on the dicarbonyl system rather than on the isolated carbonyl.

The analytical forms of the MO's remain much the same in all derivatives. Their near identity constitutes the basis of Figure 5. Alkylation of PA destabilizes all the filled MO's of Figure 5. Those orbitals with significant electron density at the nitrogens (π_5, π_4, π_3, and π_1) are affected most; the nonbonding orbitals (π_2 and all n MOs) are affected least. This preferential destabilization reverses the order of the π_4 and n_2 orbitals in DMPA relative to PA.

A correlation diagram for computed singlet states is given in Figure 6. For PA, an electric-dipole allowed $^1\Gamma_{n\pi^*} \leftarrow {}^1\Gamma_1$ transition is predicted to be of lowest energy and, from the description of the MO's which dominate this excitation (*i.e.*, n_3 and π_6^*), the excited state in question ($^1B_2$) must be associated with the dicarbonyl system. The next two lowest energy transitions are of type $^1A_2 \leftarrow {}^1A_1$ ($\pi^* \leftarrow$ n) and are electric-dipole forbidden. Although the π_5 MO is located at higher energy than π_4, the lowest energy electric-dipole allowed $\pi^* \leftarrow \pi$ transition, $^1B_1 \leftarrow {}^1A_1$, is associated with the $\pi_4\pi_6^*$ configuration; it is, rather, the next lowest energy transition, $^1A_1 \leftarrow {}^1A_1$, that involves the $\pi_6^* \leftarrow \pi_5$ excitation. Thus, the low-energy electronic absorption spectrum of PA should be dominated by three absorption regions: a low-energy $^1\Gamma_{n\pi^*} \leftarrow {}^1\Gamma_1$ absorption region of low oscillator strength and two regions of $^1\Gamma_{\pi\pi^*} \leftarrow {}^1\Gamma_1$ type at higher energy, the more energetic of which, as shown in Table V, should be the more intense.

Monomethylation reduces the symmetry of the parabanic acid system from C_{2v} to C_s. The $^1B_2(n_3\pi_6^*)$ state of MPA is predicted to red shift slightly but to remain satisfactorily describable in the single con-

figuration approximation. All transitions between π MO's have the same symmetry in the C_s point group, and, as shown in Figure 6, this circumstance allows heavy mixing of the $^1A'$ (*i.e.*, $^1B_1$ in C_{2v}) and $^1A'$ (*i.e.*, $^1A_1$ in C_{2v}) states and causes reversal of their previous order. In addition, as shown in Table V, the intensities of transitions to these states tend to equalize.

DMPA is of primitive C_{2v} symmetry and is predicted to be similar to PA in most regards. For example, despite a small predicted additional red shift of the $^1B_2 \leftarrow {}^1A_1$ transition in DMPA, the computed energy ordering and relative intensities of the two $\pi^* \leftarrow \pi$ transitions are once more expected to be similar to those for PA. However, the $^1B_1$ state is predicted to red shift considerably more than the $^1A_1$ state (0.57 *vs.* 0.33 eV, respectively), and the changes in the associated transition intensities are computed to exhibit opposite trends (a 60% decrease *vs.* a 6% increase, respectively).

The CNDO/s–CI output also includes results for triplet states. Since the exchange integral for $n\pi^*$ configurations in the CNDO/s approximation is set equal to zero, no relative energy changes are noted for the associated singlets and triplets. However, the singlet–triplet splits for $\pi\pi^*$ configurations are predicted to exhibit a considerable decrease upon dimethylation (1.97 to 1.55 eV).

Discussion

An interpretation of experiment can be attempted using: (i) generalizations[7] concerning the properties of states derived from $n\pi^*$ and $\pi\pi^*$ configurations; (ii) CNDO/s–CI computations; and (iii) a composite-molecule view of PA based on an analysis of the CNDO/s MO's. The first two approaches are used to interpret absorption and emission data of PA and its derivatives; the third view is used in order to discuss PA in terms of its relationship to simple oxamides.

Absorption. The three absorption regions of PA and its alkyl derivatives have distinctly different properties. The weak intensity, solvent shift behavior and presence of a symmetric carbonyl stretching frequency characterize[7] region I absorption as a $^1\Gamma_{n\pi^*} \leftarrow {}^1\Gamma_1$ transition. Although a solvent red shift is not observed, the increased extinction and red shift of λ_{max} upon N-alkylation serve to identify[7,8] the absorption of region III as $^1\Gamma_{\pi\pi^*} \leftarrow {}^1\Gamma^1$. The intermediate intensity of region II is not wholly characteristic of either a $^1\Gamma_{\pi\pi^*} \leftarrow {}^1\Gamma_1$ or a $^1\Gamma_{n\sigma^*} \leftarrow {}^1\Gamma_1$ transition; however, the red shifts found for N-alkylation and the solvent perturbations observed are quite characteristic of $^1\Gamma_{\pi\pi^*} \leftarrow {}^1\Gamma_1$ transitions.

The order of empirical assignments for the three lowest energy states of PA coincides with that derived from CNDO/s–CI computations (see Table V). As found previously,[1,9] the calculated energies are lower than those observed for $^1\Gamma_{n\pi^*}$ states and higher than those observed for $^1\Gamma_{\pi\pi^*}$ states. Both experiment and computation do agree, however, that the

(7) For example, see (a) M. Kasha, *Discuss. Faraday Soc.*, **9**, 14 (1950); (b) N. J. Turro, "Molecular Photochemistry," W. A. Benjamin, New York, N. Y., 1967; (c) Table 4 of ref a.

(8) E. B. Nielson and J. A. Schellman, *J. Phys. Chem.*, 71, 2297 (1967).

(9) C. J. Seliskar and S. P. McGlynn, *J. Chem. Phys.*, **56**, 1417 (1972).

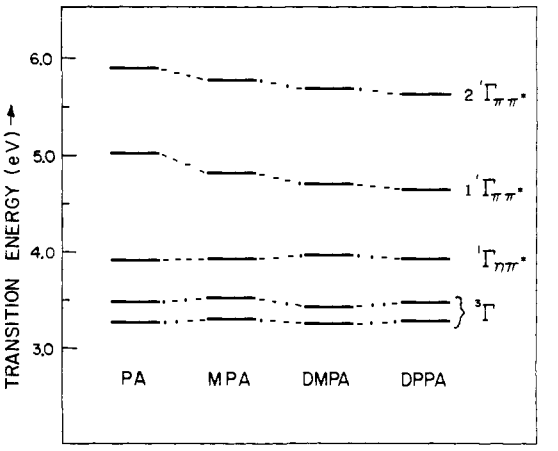

Figure 7. Correlation diagram of the experimental energies for the four lowest energy transitions of PA and its alkyl derivatives. The singlet energies represent absorption maxima in water solution for $1\,^1\Gamma_{\pi\pi^*}$ and $2\,^1\Gamma_{\pi\pi^*}$ and in ether solution for $^1\Gamma_{n\pi^*}$; the energies for $^3\Gamma$ represent the first two vibronic bands of the emissions in EPA at 77°K.

$^1\Gamma_{n\pi^*}$ ($^1B_2$) state energy of PA is only slightly affected by N-alkylation—this despite the fact that a red shift is predicted and a blue shift observed. For the two $^1\Gamma_{\pi\pi^*}$ states, the relative energy separation is calculated too large relative to experiment; however, the separation in DMPA is predicted to be larger than in PA, in agreement with experiment.

The calculated oscillator strengths for transitions to the $^1B_1$ and $^1A_1$ states of PA and DMPA correlate well with the experimental ϵ_{max} values. Relative to PA, the predicted energy shift and percentage intensity change in the DMPA $^1\Gamma_{\pi\pi^*} \leftarrow {}^1\Gamma_1$ transitions are in good agreement with experiment. For the $^1B_1 \leftarrow {}^1A_1$ transition, a 0.6-eV red shift and a 60% intensity decrease are predicted and a 0.2–0.3 eV red shift and a ~50% intensity decrease is found; for the $^1A_1 \leftarrow {}^1A_1$ excitation, a 0.3 eV red shift and a 6% intensity increase is calculated while a 0.2-eV red shift and a 6% intensity decrease is observed.

In sum, the correlation of computation with experiment is adequate to substantiate the following assignments for the three lowest energy observed singlet excited states of PA: $E[^1\Gamma_{n\pi^*}(^1B_2)] < E[1\,^1\Gamma_{\pi\pi^*}(^1B_1)] < E[2\,^1\Gamma_{\pi\pi^*}(^1A_1)]$. The noncorrelation of results for the $^1\Gamma_{\pi\pi^*}$ states of MPA, relative both to experiment and computations for PA and DMPA, is attributed to an excessive amount of CI introduced by the largely artificial point symmetry decrement $C_{2v} \rightarrow C_s$.

Emission. The emissive properties of PA and MPA mimic[7] a $^3\Gamma_{n\pi^*} \rightarrow {}^1\Gamma_1$ phosphorescence which, from the assignment of the lowest singlet, may be further described as $^3B_2 \rightarrow {}^1A_1$. The emissions found for DMPA and DPPA are not of the same character as those for PA and MPA and apparently not of $^3\Gamma_{n\pi^*} \rightarrow {}^1\Gamma_1$ origin. However, since these properties are equally incompatible with a $^3\Gamma_{\pi\pi^*} \rightarrow {}^1\Gamma_1$ assignment, the nature of the dialkyl emissions is not immediately clear.

A correlation of the experimental transition energies for the four lowest energy excited states of PA and its three alkyl derivatives is given in Figure 7. Two distinct trends correlatable to the extent of alkylation are noted: (i) the energy of the $^1\Gamma_{n\pi^*}$ state and of the $^3\Gamma$ emission remain essentially constant; and (ii) the

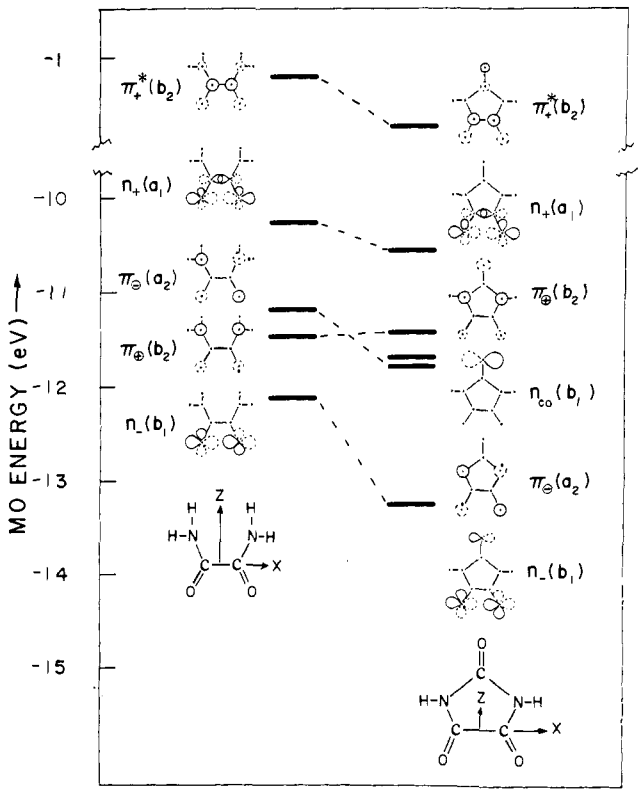

Figure 8. Correlation of MO's of PA and *cis*-oxamide. The π MO's are represented by circles and n MO's are represented by ovals; the diameter of the lobes is approximately equal to the MO coefficient at a given center. Solid lines indicate a positive MO contribution along a given axis and dashed lines a negative one.

energies of the $^1\Gamma_{\pi\pi^*}$ states progressively decrease, the $1\,^1\Gamma_{\pi\pi^*}$ state stabilizing at a faster rate than the $2\,^1\Gamma_{\pi\pi^*}$ state. Thus, the separation between the $^1\Gamma_{n\pi^*}$ and the $^1\Gamma_{\pi\pi^*}$ states decreases by $\sim$3000 cm^{-1} on going from PA to DPPA. This red shift occasioned by increasing alkylation is not linear in alkyl content, only a small stabilization being found for DPPA relative to DMPA. In view of the drastic change in emission properties caused by dialkylation as well as the observed decrease of the $n\pi^*/\pi\pi^*$ energy gap, a mixed $^3\Gamma_{n\pi^*}/^3\Gamma_{\pi\pi^*}$ state may be supposed to be responsible for the DMPA and DPPA phosphorescence properties. The predominant character of the lowest triplet in these molecules cannot be conclusively specified nor can any specific mixing mechanism be proposed. Nonetheless, whatever the mechanism, vibronic coupling in either the singlet or triplet manifold is necessary and the inverse relation between the extent of vibronic mixing and energy separation indicates that much more mixing is possible for DPPA than for PA.

Composite-Molecule Description of PA. Referring to the structure of PA given in the introductory section, one may visualize several unique partitionings of the molecule: (i) three carbonyls and two sp^2 hybridized nitrogens; (ii) two unique partitionings involving two amides and one carbonyl; (iii) one imide and one amide; (iv) urea and *cis*-glyoxal; and (v) one carbonyl and *cis*-oxamide. A convenient approach to the "best" partitioning is to correlate the MO's of PA obtained from CNDO/s calculations with those of its supposititional components i through v above. This procedure is essentially a decomposition of the MO's of PA into the MO basis sets generated by the component molecules and may be done analytically.[10] In the case of PA, however, the very characteristic forms of the MO's allow a correlation to the MO's of the residue molecules to be made on the basis of a qualitative inspection.

The two partitions urea/glyoxal [*i.e.*, iv above] and formaldehyde/oxamide [*i.e.*, v above] correlate excellently with the MO's of PA whereas other partitionings are considerably less successful. Both of these partitionings indicate that the lowest energy excited configuration (*i.e.*, $n_+\pi_+^*$) is one in which the excitation is largely localized on the dicarbonyl component of either glyoxal or oxamide fragments. The $\pi\pi^*$ configurations, however, are best described (indeed, almost uniquely so) in the formaldehyde/oxamide partitioning of PA. A detailed picture of the correlations for this partitioning, including schematic representations of the pertinent MO's, is given in Figure 8. The subscript notation used in Figure 8 for *cis*-oxamide is that which was previously found to be useful in relating the oxamides to their two constituent amides[2] and the formaldehyde notation is self-evident. The oxamide MO's that transform as C_{2v} representations for which the formaldehyde MO's do not form a basis (*i.e.*, the n_+ and $\pi_\ominus$ MO's of oxamide) remain completely oxamide like in PA. Indeed, even those MO's of oxamide which transform as C_{2v} representations for which formaldehyde MO's do form a basis (*i.e.*, the π_+^*, $\pi_\oplus$, and n_- MO's of oxamide) remain, for the most part, largely oxamide like in PA. The only exception of significance is the $\pi_\oplus$ MO which possesses a large amplitude on the isolated carbonyl oxygen; since there is no nonbonding π MO in formaldehyde with which to effect correlation, the difficulty is immediately obvious. Nonetheless, this MO is quite similar to the $\pi_\oplus(b_2)$ MO of urea and would best be treated in the urea/*cis*-glyoxal decomposition. However, the $\pi_\ominus$ MO does not correlate at all with any urea or *cis*-glyoxal MO. Thus, although the correlation given in Figure 8, based as it is on the correlation of MO's in the oxamidic portions, is not entirely satisfactory for this one $\pi_\oplus$ MO, it is superior to the urea/*cis*-glyoxal partitioning.

Based on the correlations of Figure 8, the lowest energy transitions of PA, as assigned earlier, may now be described by excited electronic configurations in which the excitation remains highly localized on the oxamide portion of the molecule: $n_+\pi_+^*$ ($^1B_2 \leftarrow {}^1A_1$ and $^3B_2 \rightarrow {}^1A_1$), $\pi_\ominus\pi_+^*$ ($^1B_1 \leftarrow {}^1A_1$), and $\pi_\oplus\pi_+^*$ ($^1A_1 \leftarrow {}^1A_1$). As emphasized, those transitions associated with the $n_+\pi_+^*$ and $\pi_\ominus\pi_+^*$ excitations are expected to be more closely related to oxamidic transitions than is the $\pi_\oplus\pi_+^*$ excitation.

The clearest validation of these predictions is provided by the vibrational modes which dominate the emission spectrum of PA. The ir–Raman analysis[5] indicates the existence of two totally symmetric carbonyl stretching modes, one involving only the dicarbonyl system and the other involving only the isolated carbonyl. The frequency found in the emission, 1780 cm^{-1}, correlates with that assigned to the dicarbonyl ground-state stretch, 1787 cm^{-1}. Furthermore,

(10) H. Baba, S. Suzuki, and T. Takemura, *J. Chem. Phys.*, 50, 2078 (1969).

the secondary frequency that occurs in this same emission may be associated with that bending mode which involves all three carbonyls but not with that one which is associated only with the isolated carbonyl. Clearly, the emission is associated with the dicarbonyl portion of PA, and the assignment made earlier, namely $^3B_2 \rightarrow {}^1A_1$, coincides with the predictions inherent in Figure 8.

A comparison of the properties associated with the $^1A_1 \leftarrow {}^1A_1$ transition (*i.e.*, the $\pi_\oplus\pi_+^*$ configuration) in *cis*-oxamide and PA shows, as expected, that the two differ in certain aspects. Although λ_{max} values are almost identical for PA and the similarly substituted *cis*-oxamide, 2,3-diketopiperazine, ϵ_{max} for PA is about twice as large as that for oxamide; alkyl substitution produces very similar red shifts but reduces the ϵ_{max} value of PA only slightly while effecting a 50% increase for the oxamide. The very limited solubility of 2,3-diketopiperazine in anything but water precludes solvent shift comparisons; however, the red shift of $\sim$1 mμ recorded for the alkyl-substituted *cis*-oxamide[2] in acetonitrile relative to water is very similar to the behavior recorded for PA and DPPA in Figure 3. A similar comparison for the $^1B_1 \leftarrow {}^1A_1$ transition (*i.e.*, the $\pi_\ominus\pi_+^*$ excitation) is not possible because the corresponding absorption[2] is ill resolved for the *cis*-oxamides.

Finally, a comparison of the emission characteristics of oxamides and parabanic acids also substantiates the importance of the $^1\Gamma_{n\pi^*}/{}^1\Gamma_{\pi\pi^*}$ separation in the determination of emission properties. The luminescence of oxamides, both cis and trans, has been rationalized[2] in terms of an emissive state of mixed $^3\Gamma_{n\pi^*}/{}^3\Gamma_{\pi\pi^*}$ character. In terms of excited electronic configurations, the union of a carbonyl and *cis*-oxamide to produce PA stabilizes the $n\pi^*$ configuration more than the $\pi\pi^*$ configurations and leads to a "pure" $^3\Gamma_{n\pi^*} \rightarrow {}^1\Gamma_1$ emission. Alkylation of PA again reduces the $n\pi^*/\pi\pi^*$ separation and, with DMPA and DPPA, emission properties which are quite similar to those of oxamides and which must also be associated with a $^3\Gamma_{n\pi^*}/{}^3\Gamma_{\pi\pi^*}$ mixed state become apparent.

Spectroscopic Studies of Lewis Acid–Base Interactions. Nuclear Magnetic Resonance Hydrogen Bonding Chemical Shifts[1a]

Frank L. Slejko[1b] and Russell S. Drago*

Contribution from the Department of Chemistry, University of Illinois, Urbana, Illinois. *Received January 8, 1973*

Abstract: Hydrogen bonding chemical shifts ($\Delta\omega^0$), defined as the difference in chemical shift between complexed and free acid, were measured for a series of hydrogen bonding Lewis acids interacting with various donors in "inert" solvents such as cyclohexane. The corresponding enthalpies of adduct formation ($-\Delta H$) were measured either calorimetrically, by the nmr technique, or calculated employing the double scale enthalpy equation: $-\Delta H = C_AC_B + E_AE_B$ (I). Linear correlations between $-\Delta H$ and $\Delta\omega^0$ were obtained for a given base interacting with a series of hydrogen bonding Lewis acids when the base was quinuclidine, tetrahydrothiophene, or 1-phospha-2,6,7-trioxa-4-ethylbicyclo[2.2.2]octane. Similar linear relationships could not be established when the base was acetonitrile, tetrahydrofuran, and diethyl ether or when the base contained strongly magnetically anisotropic groups as with pyridine or acetone. In light of the lack of generality for a constant base $-\Delta H$ *vs.* $\Delta\omega^0$ correlation, the $\Delta\omega^0$ values were accounted for in terms of an electric field model based on one originally proposed by Buckingham: $\Delta\omega^0 = K\alpha_{||a}E_B^2$ (II), where $\alpha_{||a}$ is the polarizability of the acid along the X–H bond and E_B is some "average" electric field originating on the lone pair electrons of the donor. The values of $\alpha_{||a}$ for the acids studied here were obtained from their corresponding C_A and E_A parameters appearing in eq I. For a given base interacting with a series of acids for which $\alpha_{||a}$ values were available, a linear relationship was obtained when $\Delta\omega^0$ was plotted *vs.* $\alpha_{||a}$. In all cases, except where the base contributed appreciably to $\Delta\omega^0$ from its neighbor anisotropy effect, a straight line resulted, even where no linear ΔH *vs.* $\Delta\omega^0$ constant base relationship could be established. From the slopes of these $\Delta\omega^0$ *vs.* $\alpha_{||a}$ plots, the "average" electric fields for the bases were obtained using eq II. The information about these donor "average" electric fields was found to be incorporated in their corresponding C_B and E_B parameters of eq I. Utilizing eq I and II, the linear $-\Delta H$ *vs.* $\Delta\omega^0$ correlations and their exceptions were accounted for, either when the base was kept constant and the acid varied, or when the acid was kept constant and the base varied.

It has been well established that the position of a hydrogen bonded proton in a nmr spectrum is different from the position of the "free" proton.[2] The resonance usually shifts to lower field unless the donor involved in the hydrogen bonding interaction has a large magnetic anisotropy. Benzene is such a donor and causes a net upfield shift in the hydrogen bonded proton upon adduct formation.

The hydrogen bonding chemical shift, $\Delta\omega^0$, defined as the difference in chemical shift between complexed

(1) (a) Abstracted in part from the Ph.D. Thesis of F. L. Slejko, University of Illinois, Urbana, Illinois, Aug 1972. (b) National Science Foundation Predoctoral Fellow, 1969–1972.

(2) See, for instance, J. W. Emsley, J. Feeney, and L. H. Sutcliffe, "High Resolution NMR," Pergamon Press, Oxford, 1965.